X-911-76-147

PREPRINT

EARTH-ATMOSPHERE SYSTEM AND SURFACE REFLECTIVITIES IN ARID REGIONS FROM LANDSAT MULTISPECTRAL SCANNER MEASUREMENTS

J. OTTERMAN
R.S. FRASER

JUNE 1976

GSFC
GODDARD SPACE FLIGHT CENTER
GREENBELT, MARYLAND

X-911-76-147

EARTH-ATMOSPHERE SYSTEM AND SURFACE REFLECTIVITIES IN ARID REGIONS FROM LANDSAT MULTISPECTRAL SCANNER MEASUREMENTS

J. Otterman
R. S. Fraser

June 1976

GODDARD SPACE FLIGHT CENTER
Greenbelt, Maryland

EARTH-ATMOSPHERE SYSTEM AND SURFACE REFLECTIVITIES IN ARID REGIONS FROM LANDSAT MULTISPECTRAL SCANNER MEASUREMENTS

J. Otterman*
R. S. Fraser**

ABSTRACT

Previously developed programs for computing atmospheric transmission and scattering of the solar radiation are used to compute the ratios of the Earth-atmosphere system (space) directional reflectivities in the vertical direction to the surface reflectivity, for the four bands of the Landsat multispectral scanner (MSS). These ratios are presented as graphs for two water vapor levels, as a function of the surface reflectivity, for various sun elevation angles. Space directional reflectivities in the vertical direction are reported for selected arid regions in Asia, Africa and Central America from the spectral radiance levels measured by the Landsat MSS. From these space reflectivities, surface vertical reflectivities are computed applying the pertinent graphs. These surface reflectivities are used to estimate the surface albedo for the entire solar spectrum. The estimated albedos are in the range 0.34-0.52, higher than the values reported by most previous researchers from space measurements, but are consistent with laboratory measurements.

*Tel-Aviv University, Department of Geophysics & Planetary Sciences, Ramat Aviv, Israel, Currently National Academy of Sciences, National Research Council Research Associate at NASA/Goddard Space Flight Center, Greenbelt, Md.
**NASA/Goddard Space Flight Center, Greenbelt, Maryland.

CONTENTS

ILLUSTRATIONS

*The parametric curves are shown for four values of the solar zenith angle.

TABLES

INTRODUCTION

A strong impact on the surface albedo has been observed and reported as being due to overgrazing, cultivation and other anthropogenic pressures in the arid region of the Sinai-Negev demarcation line (Otterman, 1973; Otterman et al., 1974). Such an impact was found to exist in other arid regions, such as the Kara Kum region in the USSR and the neighboring Afghanistan and in the Sahel region of Africa (Otterman et al., 1976). All these observations were based on the imagery taken by the Landsat multispectral scanner (MSS). In the last of these studies contrast ratios were computed between the bright areas of denuded soil and the darker, protected areas of natural vegetation from the MSS computer compatible tapes, i.e., the digitized imagery. The absolute values of albedo were not reported in any of these studies.

In this paper the values of the spectral reflectivities in the vertical direction, for some selected sites in arid regions are computed, from the measurements of the upward radiances by the Landsat MSS. Results of computed atmospheric transmission and scattering are first presented in terms of the ratio between the upward reflectivity as seen from space (i.e., Earth-atmosphere system reflectivity) and the ground (i.e., surface) reflectivity, for various solar elevation angles and various atmospheric models. Using these ratios, the ground reflectivities are computed from the space reflectivities, assuming atmospheric conditions. These results are presented with an assessment of expected accuracy.

SPACE REFLECTIVITY TO SURFACE REFLECTIVITY RATIOS COMPUTED FOR ATMOSPHERIC MODELS

Dave (1970a; 1970b) and Dave and Gazdag (1970) developed programs for computing atmospheric transmission, scattering and absorption of the solar radiation, assuming a plane-parallel atmosphere containing the standard dry atmospheric gases, water vapor and arbitrary vertical distributions of ozone and aerosol number-density. The model atmosphere is bounded at the Earth's surface, which is assumed to reflect the incident radiation according to Lambert's law. The scattering aerosols are assumed to be spherical particles made up of a homogeneous material with a known refractive index. This refractive index and the size distribution function are independent of height.

The irradiation at the top of the atmosphere is assumed to be unidirectional, unpolarized and monochromatic. The intensity and the scattering phase functions are expressed as Fourier series in which the azimuth is the argument. As a result, the equation of radiative transfer for the intensity reduces to a integro-differential equation with the polar angle and the vertical optical thickness as independent variables. This equation for the intensity is solved numerically until the intensities at selected levels in the atmosphere in successive iterations differ by less than 0.2%.

The computations can be carried out at two levels of complexity. At the more detailed level, the polarization characteristics of radiation scattered by the multiple scattering are taken into account. However, because of the excessive complexity and the computer time requirements, a simplified approach,

which does not account for detailed polarization aspects, was used here. Neglect of polarization results in intensity errors of less than 2% for the atmospheric models used here.

The radiance of the light emerging vertically upward from the top of the atmosphere was computed for these parameters:

Spectral bands:	MSS-4 (0.5-0.6 μm); MSS-5(0.6-0.7 μm); MSS-6 (0.7-0.8 μm); MSS-7(0.8-1.1 μm)
Solar zenith angle;	30°; 40°; 50°; 60°
Ground albedo;	0.1; 0.2; 0.3; 0.4; 0.5
Aerosol characteristics:	Index of refraction, m = 1.5 number density law:

$$n(r) = \text{constant}, \quad 0.03 \leq r \leq 0.1 \ \mu m$$

$$n(r) = \text{constant } r^{-4}, \quad 0.1 \leq r \leq 10.0 \ \mu m$$

where n(r) is the number of particles per cubic centimeter per micrometer of radius of the particles.

Two particle concentrations are used, and the total optical depth is as follows:

Concentration I - total number of particles in a vertical column 3.24×10^8, which results in an aerosol optical thickness of 0.199 at 0.55 μm. Turbidity, defined as the ratio of the total vertical optical thickness (aerosol, Rayleigh and ozone) to the Rayleigh value (0.098) at this wavelength, is 3.3.

Concentration II - total number of particles in a vertical column 6.48×10^8, which results in an aerosol optical thickness of 0.398 at 0.55 μm. Turbidity, as defined above, is 5.3.

The vertical distribution of the aerosols is as given by Bahethi and Fraser (1975), which has a scale height of 0.8 km for the lowest 5 km. Scattering is computed for the mid-band values of the MSS bands, i.e., for 0.55, 0.65, 0.75 and 0.9 μm, respectively, in the four bands. Absorption effects are computed as an average for the band and not specific to any wavelength. Water vapor absorption is quite significant in band MSS-7. Two values for water vapor are used, 10 and 29 mm in a vertical column.

Kondratyev et al. (1974) used both data from the ground measurements of the surface albedo, A_0, and data from satellite measurements of space albedo (top-of-the-atmosphere, on Earth-atmosphere system albedo), A_S, to tabulate the ratio A_S/A_0. This approach was used by Lettau and Lettau (1969; 1972). A similar approach is followed here and the 200 computed data points are presented as a ratio of Earth-atmosphere system spectral reflectivity, a_S, to ground reflectivity, a_0, plotted versus the ground reflectivity, with the solar zenith angle as a parameter. The space reflectivity is defined as

$$a_{s\lambda} = \frac{\pi N_\lambda}{\cos \theta_0 S_\lambda} \tag{1}$$

where N_λ is the radiance of the nadir for any of the four MSS bands and (cos θ_0 S_λ) is the incident irradiance in the same band through a horizontal surface at the top of the atmosphere. In what follows the subscript λ is omitted.

The ground reflectivity $A_{0\lambda}$ as assumed in the models for the Earth's surface, is defined as

$$a_{0\lambda} = \frac{\pi N_{0\lambda}}{G_\lambda} \tag{2}$$

where $N_{\lambda 0}$ is radiance coming from the ground and G_λ is the global irradiance incident on the ground. Because the ground is assumed to be a Lambert reflector, $N_{\lambda 0}$ is independent of the direction of the incident radiation, G_λ. Moreover, $N_{0\lambda}$ and therefore $a_{0\lambda}$ is independent of the direction from which the ground is observed.

The results are presented in Figures 1-4 respectively for the 4 spectral bands, for the 3.3 turbidity, where in Figure 4 for MSS-7, 10 mm water vapor is assumed. In Figure 5, the ratios for MSS-7 are repeated for 29 mm amount of water vapor. Those two amounts of water vapor bracket the more commonly found levels in arid regions (Joseph, 1975). In Figures 6-10 similar graphs are given for the 5.3 turbidity.

It can be seen from Figures 1-10, that the space reflectivity does not differ very significantly from the surface reflectivity when the ground reflectivities are in the range 0.2-0.5, as noted by Kondratyev et al. (1974) for the albedo. Band MSS-7, infrared, constitutes as exception. In that band the space reflectivity, depending on the water vapor levels, can be significantly lower than the surface reflectivity.

As pointed out by Kondratyev et al. (1974), the knowledge of the relationship between the surface albedo and the space albedo is important for treatment of Earth's radiation balance components. For such a purpose an accurate treatment of absorption, separately by the surface and by the atmosphere at various levels, as a function of the sun elevation angle is mandatory. These absorption components can be computed from the computer programs discussed above, but such computations are not presented here. The purpose of the paper is to point out the large uncertainties that exist in the values of surface albedo of arid regions, and to report new measurements of spectral reflectivities for well defined cloud-free areas, areas which are much smaller than be selected in studies from the low resolution meteorological satellites.

COMPUTATION OF SPACE UPWARD REFLECTIVITY FROM LANDSAT MULTISPECTRAL SCANNER MEASUREMENTS

The multispectral scanners of Landsat-1 and 2 are essentially identical instruments operating in 4 spectral bands. For details see NASA (1971). The radiances measured by MSS are digitized in the spacecraft and transmitted to the ground in a digital form. There are 128 levels in bands MSS 4, 5 and 6 and 64 levels in MSS 7. The radiances corresponding to the minimum and maximum digitized reading in each spectral band are presented in Table 1. The radiance is a linear function of the digitized values for each band.

For calibration procedures, and the characteristics of MSS data, see Grebowsky (1975). As part of Landsat MSS calibration procedures, repeated readings are taken for two sandy desert areas in northern Mexico near the Colorado River. These readings were converted into upward radiance, N_λ, linearly, in accordance with the data given in Table 1. The upward space reflectivity a_s was subsequently computed from Eq. (1).

Following calculation of a_s, from the Landsat data, the ratio a_s/a_0 is read off from graphs given in Figures 1-10, i.e., turbidity 3.3 or 5.3, in band MSS-7 10 mm or 29 mm water vapor, interpolating for the solar zenith angle. In the first iteration, the abscissa value of a_o is assumed to be numerically equal to the space derived a_s. A value of a_o is obtained from a_s, dividing a_s by the a_s/a_o ratio from the appropriate graph. This first estimate of a_o is used to obtain a new reading of the a_s/a_o ratio, and a new calculation of a_o. One iteration is

enough for bands MSS-4, 5 and 6, but two are required for MSS-7. The results for the two areas in northern Mexico are presented in Table 2.

Examining the contents of Table 2, one can conclude that the repeatability of the MSS measurements is quite satisfactory and that the variability of the reflectivities at different dates and solar zenith angles typically amounts to only about 0.01 (or about ±3% of the magnitude of the reflectivity). Moreover it can be noted that for the bands MSS-4, 5 and 6, the ratios a_s/a_o are quite close to unity for both 3.3 and 5.3 turbidities, and the changes in aerosol loadings for such non-absorbing aerosols do not affect materially the computation of the ground reflectivities, for ground reflectivity values in the range 0.2 - 0.4. Such confidence is not justified for band MSS-7, where lack of information about the water vapor level at the time of the observation introduces a large uncertainty.

From the computer compatible digital tapes of the Negev and the Sinai, the MSS readings or counts were taken using General Electric Image 100 Analyzer. The readings were taken from three pairs of points, or rather small sampling areas, one site just inside the Negev and one just inside the Sinai. The first pair was selected close to the point where the Negev, the Sinai and the Gaza Strip meet in the vicinity of Kerem Shalom and the other sites, #2 and #3, were progressively more inland from the Mediterranean, where the soil becomes more sandy (the Sands of Haluza). Two sets of data were obtained from October 22, 1972 and January 2, 1973. The same type of readings were taken for the Sahel (inside and outside a ranch), for the Kara Kum region of the Soviet Union

and the neighboring Afghanistan, for the Thar desert in India and for the Western coast of Africa and the Libyan desert areas. The space reflectances are tabulated Table 3. The a_s/a_o ratios were read off from Figs. 1-4, i.e., only the turbidity of 3.3 and the 10 mm water vapor level in MSS-7, were used. The computed values of a_o are also tabulated in Table 3. The tabulated infrared ground reflectivities in MSS-7 can be regarded as a low estimate of the actual reflectivity, since they are computed using very high,(i.e., relatively close to one) a_s/a_o ratios, corresponding to the lowest likely water vapor levels.

ASSESSMENT OF RESULTS

The high values of the reflectivity in the infrared for sandy areas in arid regions, in many cases exceeding 50%, are surprising, but credible in view of laboratory measurements of reflectivity performed by W. A. Hovis. He observed for the spectral band 0.8 to 1.1 μm reflectivities of: 55% for Daytona Beach sand of grain size 0.105 to 0.250 mm; 55% for gray clay, Bad Water desert, Death Valley, California; 58% for Red Sandstone, ground, less than 0.038 mm; 62% for silica sand less than 0.105 mm; 66% for silica sand, 0.105 to 0.250 mm and 63% for silica sand 0.25 to 0.5 mm. These values higher than 50%, compare with 42% for Atlantic City, N. J., beach sand; 45% for Daytona Beach sand, 0.250 to 0.5 mm; 43% for gypsum sand, White Sands, New Mexico; 38% for Mojave Desert Soil (Hovis, 1966; Hovis, 1975). Leeman et al. (1971) also report high values of infrared soil reflectivity, higher than 50% for many types of soil.

In the winter and spring of 1976, reflectivity measurements were carried out of the Sinai/Negev terrain components: crumbled Sinai #1 soil, plant debris, Sinai #1 crusted soil and of a prevalent plant, Artemesia monosperma. The measurements were taken in-situ, using EXOTECH-100 radiometer, which operates in the Landsat bands. The results are presented in the first five lines of Table 4. In the following four lines, the reflectivities of Sinai #1 and Negev #1 are retabulated from Table 3 for convenience of comparison (the numbers are rounded off to two significant digits). It can be seen that the measured reflectivities of Sinai #1 crumbled soil overall are very close

to the terrain reflectivities of Sinai #1 - which, by ground truth observations, indeed consists largely of overgrazed, trampled soil. There is a notable discrepancy only in the band MSS-6 : 0.50 measured from Landsat is certainly much higher than 0.40 measured in-situ.

Since the soil type does not vary from one side to the other of Sinai/Negev boundary, the low reflectivities of Negev #1 terrain (if shadowing effects of vegetation clumps are neglected) can be explained only by a predominant darkening role of plant debris scattered on the surface.

The measured reflectivities in the bands MSS-7 and MSS-6 were used to estimate the reflectivity of the complete infrared portion of the solar spectrum (see Table 5). The infrared reflectivity was calculated as the sum of reflectivity in band MSS-6 and 3 times reflectivity in band MSS-7, divided by four. At wavelengths longer than 1.1 μm still are found 26 percent of the solar spectrum, and thus the reflectance characteristics in this region, which are not measured, are a source of uncertainty in computing the albedo. But examination of reflectivity vs. wavelength curves (Hovis, 1966; Hovis, 1975; Leeman et al. 1971) does not indicate any sharp drop or rise of reflectivity of soils above 1.1 μm. A significant drop of reflectivity can be observed for some types of soils only above 2.5μm, but above that wavelength no more than 6 percent of the solar energy are found. The measured reflectivities in the bands MSS-4 and MSS-5 weighed 2:1, were used to calculate the visible reflectivity.

The infrared irradiation constitutes somewhat less than 50% of the total incident solar irradiation at the top of the atmosphere and can be more than 50% at the ground, depending on the water vapor levels. For 20 mm of precipitable water, the infrared fraction is 50% for one airmass, i.e., sun at the zenith and increases with an increasing solar zenith angle, becoming 61% for five airmasses (Smithsonian Meteorological Tables, 1958, p. 438). Weighting the visible and infrared reflectivities equally, we obtain an approximate albedo a_0 average for all wavelengths for high solar elevations.* We summarize the albedo calculations in Table 5.

The computed albedo of 0.47 - 0.52 as an effective average for all wavelengths at the ground level for Sinai, Site #3, is much higher than the results of Kondratyev et al. (1974). They reported surface albedo of 0.28 - 0.32 for the Arabian peninsula and 0.21 - 0.30 for Sahara. Pytovskaya (1974) reported albedo measurements from Cosmos 144 and 184 over Sahara in the 0.3 - 3.0 μm region ranging from 0.23 and 0.36. Kung et al. (1974) reported albedo values from aircraft measurements of beam albedo** within this range: Sonora Desert, S. Arizona, 0.22; Desert near Yuma, S. E. California, 0.27 - 0.28; Desert near Las Vegas, S. E. Nevada, 0.24 - 0.27. The measurements by Bryson over the Thar desert in India were in the 0.20 - 0.22 range (Bryson, 1974).

*For accurate computation, the effective surface albedo should be calculated as a function of time of day, season, latitude and meteorological conditions. For 10 mm of precipitable water, the infrared fraction would be higher than in the case for 20 mm.

**Kung et al. (1964) define beam albedo as an albedo derived from measuring the downward stream of solar radiation by a 2π steradian upward viewing instrument and the reflected radiation by a narrow beam (4° in their case) instrument. They subsequently convert their measured beam albedo to hemispheric albedo.

Budyko (1974) tabulated measurements from many sources and reports on the one hand an albedo of 0.35-0.45 (Table 6; p. 54) for dry light sandy soils, but on the other a single value of 0.28 for desert (his Table 7 of more broadly averaged values, recommended for use in schematic climatological calculations, p. 55). Budyko's value of 0.28 for deserts would agree well with the results of Kondratyev et al. (1974), but Budyko's high range for dry light sandy soils comes close to our values.

Why do such large differences exist in the reported values of albedo? Budyko (1974) points out that albedo of various surfaces varies with time of day and seasons and is higher in the morning and evening hours than at midday. Landsat operated at nearly fixed mid-morning time of about 0930 hours. But this effect is nearly certainly, at most, only a partial explanation. The source of the differences might lie in much higher reflectivity in the infrared than in the visible, and the older measurements possibly did not fully account for the infrared contribution.

The radiometric accuracy of Landsat MSS cannot be firmly assessed at this time, but in view of detailed pre-flight calibration and no indication of any strong drift in the operation, probably is about 10%. The sun elevation angle in a MSS frame varies by 0.009°/km along the solar azimuth, from the image center, and the small departures from the sun elevation at the frame center were neglected.

The values of effective albedo, as tabulated in Table 5, might actually be regarded as lower limits of actual albedo for these reasons:

(a) In weighing the infrared as only 50% of the surface irradiance, we approximate the albedo on the low side, for high solar elevation conditions. If the infrared reflectivity is weighed more heavily, a higher effective albedo would result for all measurements reported here, since the infrared reflectivity is significantly higher than the visible reflectivity. For instance, the effective albedo for Sinai #1 winter becomes 0.44 rather then 0.41, if the infrared fraction at the ground of 61% is assumed.

(b) An assumption is made of a Lambertian reflection at the surface. Any specular reflection component or backward reflection from the ground would not be detected in our measurements of the vertical radiances and reflectivities, and would increase the actual albedo. Such effects can be non-negligible, as observed in laboratory measurements (Coulson et al., 1965; Salomonson, 1968).

(c) The a_s/a_0 ratios were calculated assuming non-absorbing aerosols. An assumption of absorbing aerosols (imaginary component of the index of refraction) results in lower a_s/a_0 ratios, i.e., higher values of a_0 for a space-derived a_s.

(d) In many arid areas, such as the Negev, vegetation grows in isolated clumps with twigs and stalks mostly vertical. Such structure can result in some shadowing effects, which reduce the vertical reflectivity but not necessarily the overall albedo.

Wexler (1958) in his study of the artificial climate modification, discusses reducing the albedo of the deserts by a factor of 2. He assumed the albedo of deserts to be 0.25-0.30. If it is actually about 0.45, the effects he discusses would be greater by 50% to 80%. Otterman (1974) suggested that the effects on Earth's radiation balance (assuming no climatic feedback) of overgrazing in the Sahel were of the same order of magnitude as the effects of shifts in the ice

cover. The assumptions were: 0.37 as the albedo of bare soil and 0.25 as the albedo of steppe areas, for 0.12 difference in albedo. As seen in Table 3, ratios of reflectivity between the overgrazed areas and the protected areas can be as high as a factor of 2. For albedo values approaching 0.50, the difference in albedo can be over 0.20 and the effects as discussed by Otterman (1974) would be by two thirds larger.

There is one more significance of this type of measurement. Some meteorological satellites carry radiometer which measure with a poor spatial resolution, but high radiometric accuracy, the broad band (0.4-3 micrometers) solar radiation. However, such radiometers do not have a response flat in wavelengths – (see Raschke et al., 1973), and an assumption has to be made about the spectral distribution of the incoming radiation in order to interpret the radiometer measurements. Here, this type of spectral distribution for some arid regions is presented.

Continued measurements of surface albedo are certainly warranted. Most previous measurements possibly did not take properly into account the high infrared reflectivity of some terrain types. As a result surface albedo of continental areas has been underestimated. It appears worthwhile to undertake seasonal mapping of spectral reflectivities and albedo of land areas as a climatological record. The use of high-resolution, multi-spectral and repetitive coverage Landsat-type satellites as suggested. Even though for a climatological record the high resolution (80 m) of Landsat is not needed, such high resolution offers the capability to avoid small clouds and to carry out gross thematic mapping of terrain type. Typifying the terrain makes it possible to introduce a correction for non-Lambertian surface reflectance, based on field

measurements of this effect for a particular terrain. When a change in surface characteristics is observed, thematic mapping can most of the time indicate what is the change, whether the change is strictly temporary, for instance soil moisture after a rainfall or an inundation, or a more permanent change, as for instance irrigating an arid area. In view of the importance of accurately monitoring surface albedo, the large scale data processing effort needed appears to be justifiable.

ACKNOWLEDGEMENTS

We gratefully acknowledge calculations by O. Bahethi, Computer Science Corporation, M. Smith, NASA, and L. Rudolf, New York City University.

REFERENCES

Bahethi, O. P. and R. S. Fraser (1975), Effect of Molecular Anisotrophy on the Intensity and Degree of Polarization of Light Scattered from Model Atmospheres, NASA, Goddard Space Flight Center Report X-910-75-52.

Bryson, R. A. (1974), private communication.

Budyko, M. I. (1974), Climate and Life, Academic Press, New York and London.

Coulson, K. L., G. M. B. Bouricius, and E. L. Gray (1969), Effects of Surface Reflection on Radiation Emerging from the Top a Planetary Atmosphere, GE Missile and Space Division, R65SD64.

Dave, J. V. and J. Gazdag (1970), A Modified Fourier Transform Method for Multiple Scattering Calculations in a Plane-Parallel Mie Atmosphere, Applied Optics, 9, 1457-1466.

Dave, J. V. (1970a), Intensity and Polarization of the Radiation Emerging from a Plane-Parallel Atmosphere Containing Monodispersed Aerosols, Applied Optics, 9, 2673-2684.

Dave, J. V. (1970b), Coefficients of the Legendre and Fourier Series for the Scattering Functions of Spherical Particles, Applied Optics, 9, 1888-1896.

Grebowsky, G. J. (1975), Characteristics of Digital Multispectral Scanner Data, NASA, Goddard Space Flight Center Report X-563-75-169.

Joseph, J. H. (1975), Tel Aviv University, private communication.

Hovis, W. A., Jr. (1966), Infrared Spectral Reflectance of Some Common Minerals, Applied Optics, 6, 245-248.

Hovis, W. A., Jr. (1975), private communication.

Kondratyev, K. Ya., L. N. Dyachenko, and N. P. Piatovskaya (1974), On the Relationship Between the Earth-Atmosphere System Albedo and the Earth's Surface Albedo, in Earth Survey Problems, Akademie-Verlag, Berlin, 473-482.

Kung, E. C., R. A. Bryson, and D. H. Lenschow (1964), Study of a Continental Surface Albedo on the Basis of Flight Measurements and Structure of the Earth's Surface Cover Over North America, Monthly Weather Review, 92, 543-564.

Leeman, V., D. Earing, R. K. Vincent, S. Ladd (1971), The NASA Earth Resources Spectral Information System: A Data Compilation, NASA CR-WRL-31650-24-T.

Lettau, H. and K. Lettau (1969), Shortwave Radiation Climatonomy, Tellus 21, 208-222.

Lettau, H. and K. Lettau (1972), Manual to Calculate Climatic Time Series of Global and Diffuse Radiation Based on Concepts of Shortwave Radiation Climatonomy, University of Wisconsin Report.

NASA (1971), Data Users Handbook, Earth Resources Technology Satellite, GSFC Document 71504249.

Otterman, J. (1973), Preliminary Results from Israeli ERTS-1 Program, Rassegna Internazionale Elettronica Nucleare ed Aerospaziale, XX, 199-203.

Otterman, J. (1974), Baring High-Albedo Soils by Overgrazing: A Hypothesized Desertification Mechanism, Science, 186, 531-533.

Otterman, J., G. Ohring, and A. Ginzburg (1974), Results of the Israeli Multidisciplinary Data Analysis of ERTS-1 Imagery, Remote Sensing of Environment, 3, 133-148.

Otterman, J., L. S. Walter, and T. S. Schmugge (1976), Observations from ERTS of Overgrazing and Cultivation Impact on the Earth's Surface, Space Research XVI, 15-21.

Pyatovskaya, N. P., (1974), Albedo of the Earth-Atmosphere system for Clear and Overcast Skies, in Atmospheric Radiation Studies, K. Ya. Kondratyev, Israel Program for Scientific Translations, Jerusalem 14-27.

Salomonson, V. V., (1968), Anisotrophy in Reflected Solar Radiation, Atmospheric Science Paper No. 128, Colorado State University.

Smithsonian Meteorological Tables, (1958) prepared by R. J. List, Publication 401, the Smithsonian Institution.

Raschke, E., T. H. Vonder Haar, M. Pasternak, and W. R. Bandeen (1973), The Radiation Balance of the Earth Atmosphere System from NIMBUS-3 Radiation Measurements, NASA Technical Note TN D-7294, April 1973.

Wexler, H. (1958), Modifying Weather on a Large Scale, Science, 128, 1059-1063.

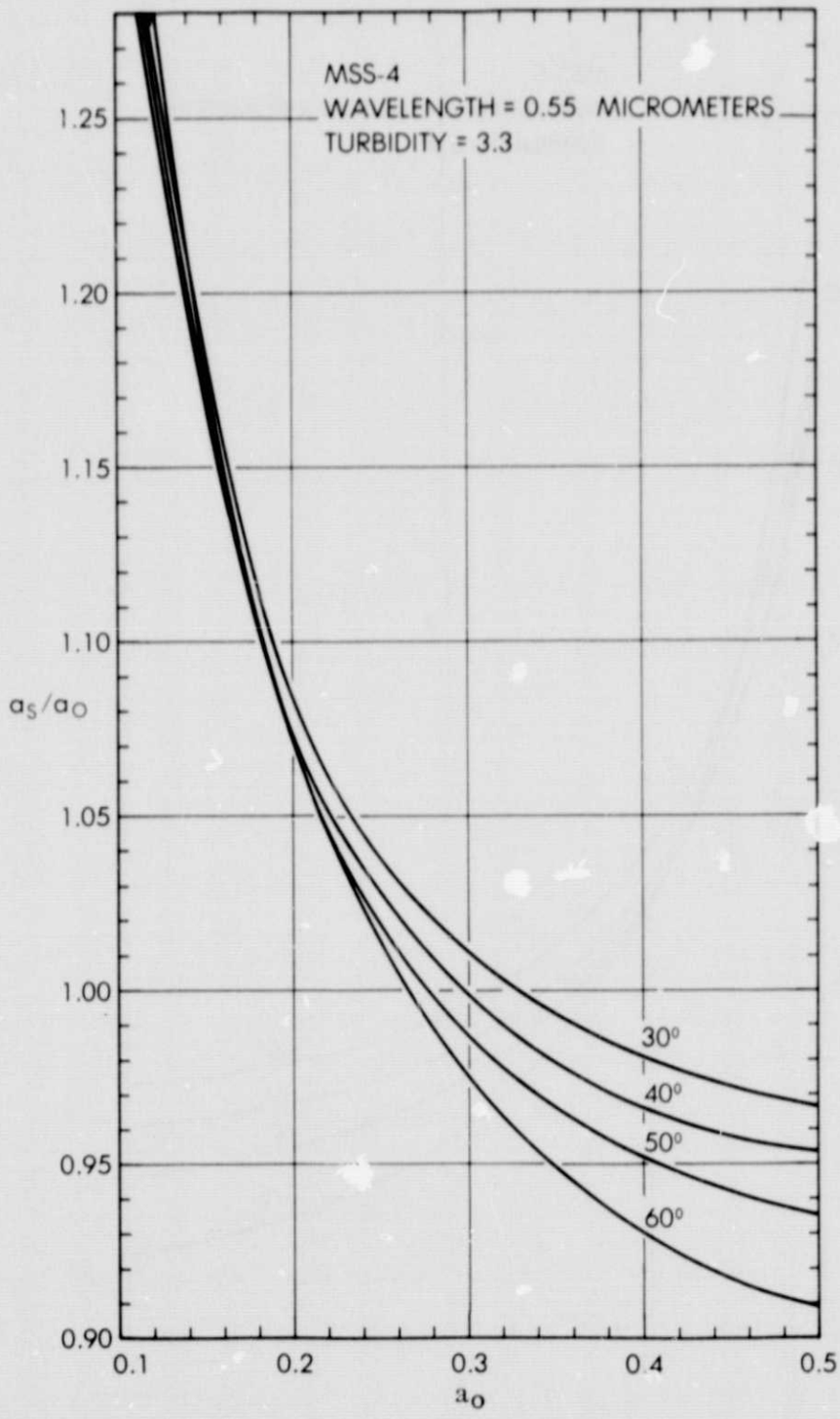

Fig. 1. The space reflectivity to ground reflectivity ratios a_s/a_0 vs ground reflectivity a_0, Band MSS-4, turbidity 3.3. The parametric curves are shown for four values of the solar zenith angle.

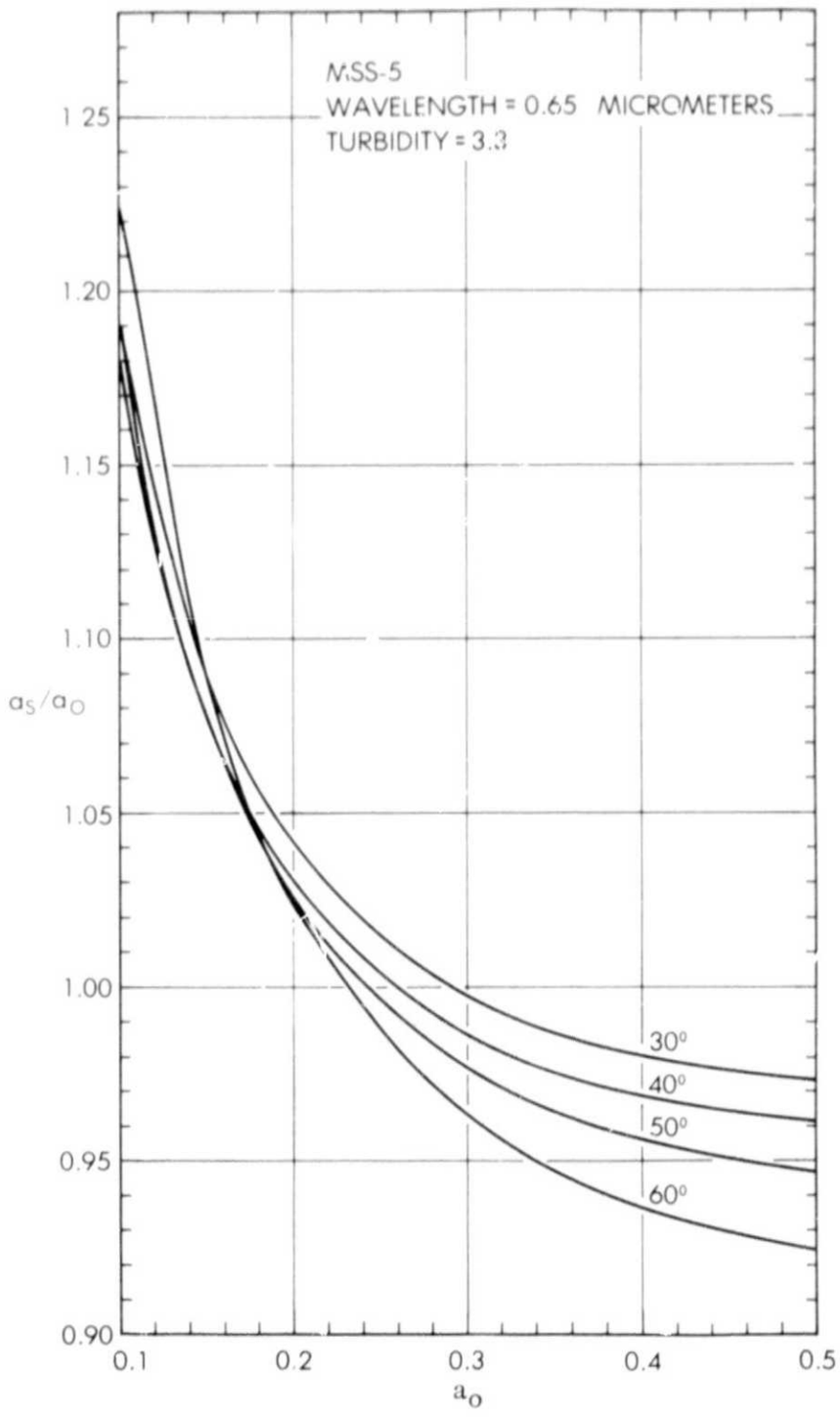

Fig. 2. The space reflectivity to ground reflectivity ratios a_s/a_0 vs ground reflectivity a_0, Band MSS-5, turbidity 3.3. The parametric curves are shown for four values of the solar zenith angle.

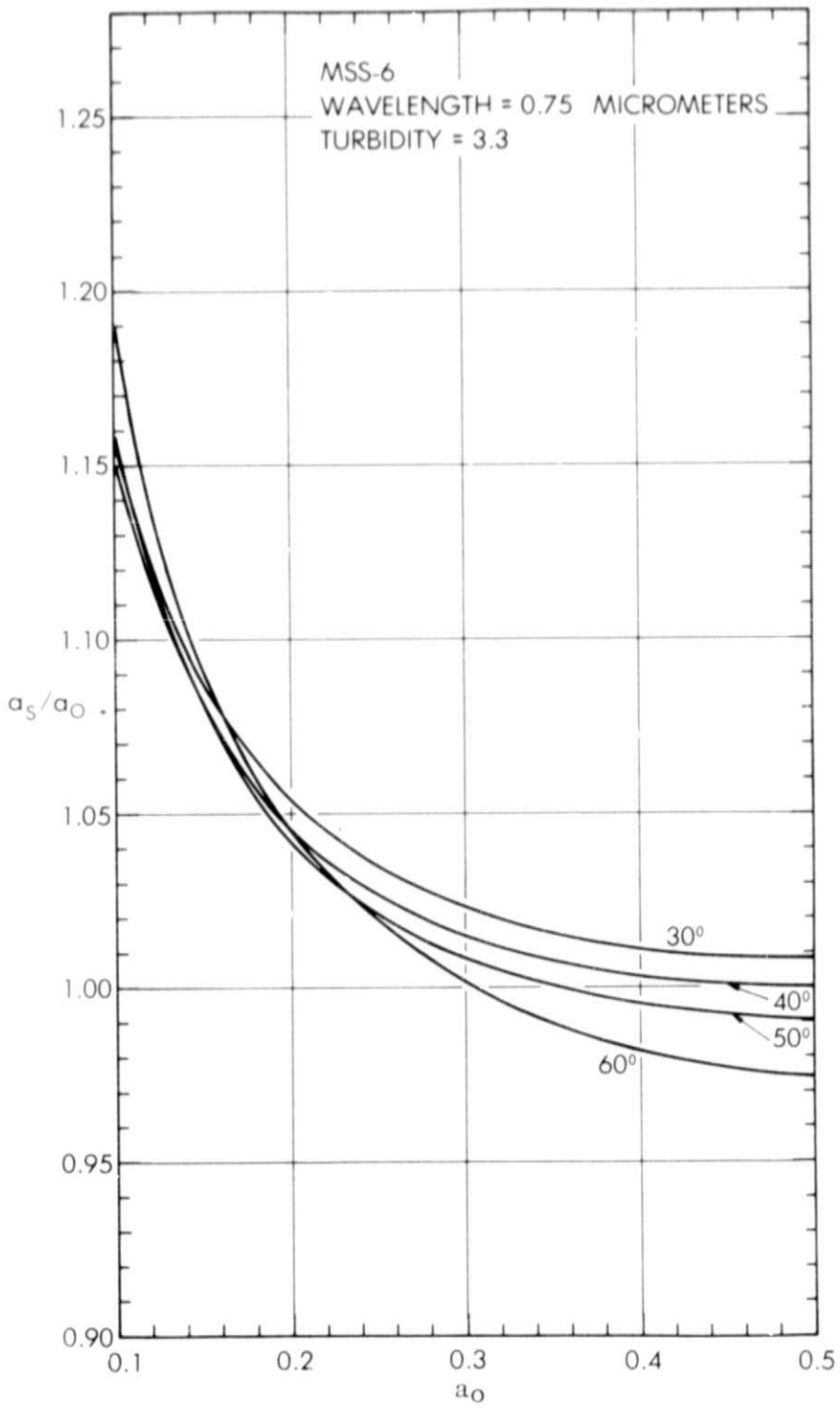

Fig. 3. The space reflectivity to ground reflectivity ratios a_s/a_0 vs ground reflectivity a_0, Band MSS-6, turbidity 3.3. The parametric curves are shown for four values of the solar zenith angle.

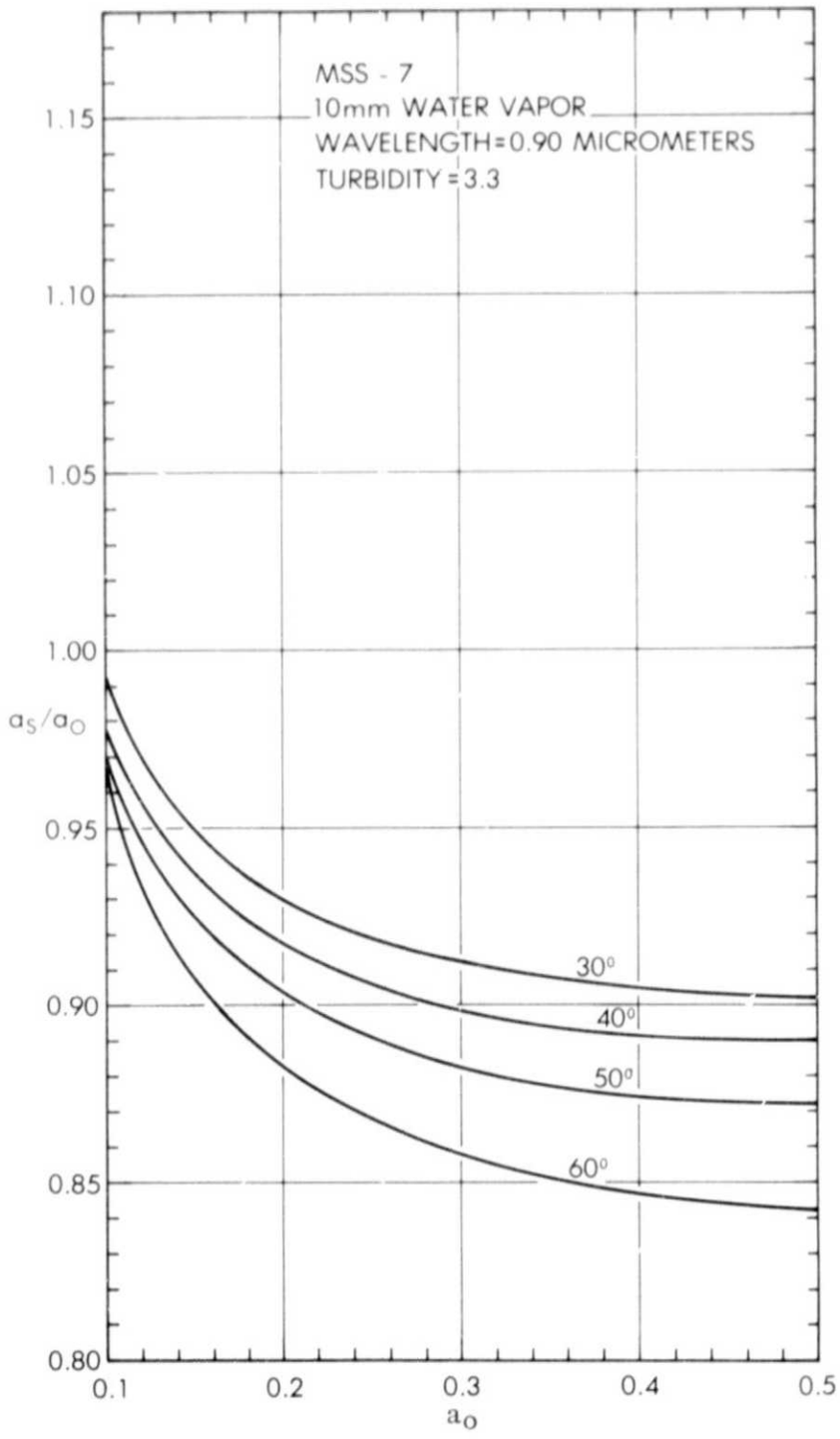

Fig. 4. The space reflectivity to ground reflectivity ratios a_s/a_0 vs ground reflectivity a_0, Band MSS-7, turbidity 3.3, water vapor 10 mm. The parametric curves are shown for four values of the solar zenith angle.

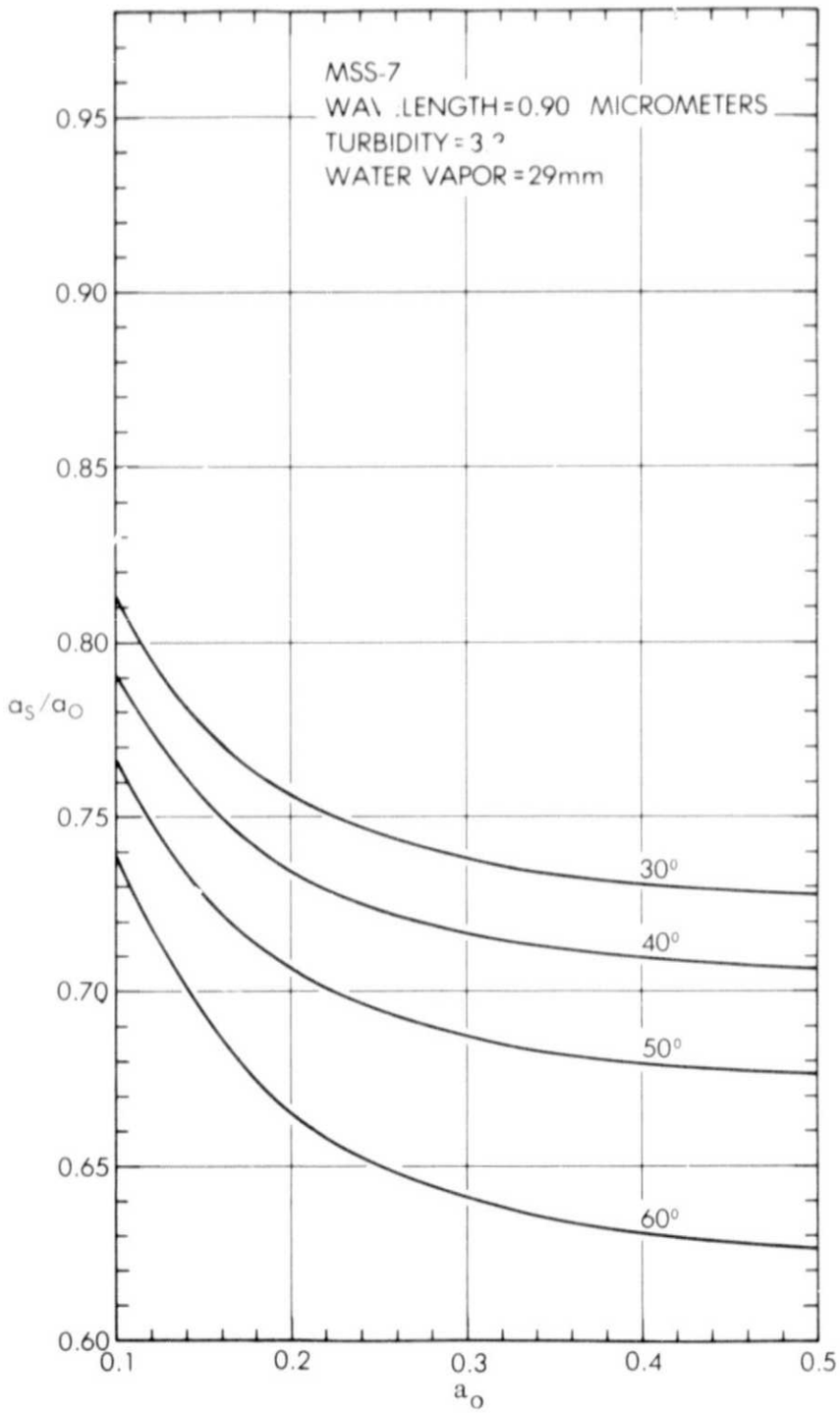

Fig. 5. The space reflectivity to ground reflectivity ratios a_s/a_0 vs ground reflectivity a_0, Band MSS-7, turbidity 3.3, water vapor 29 mm. The parametric curves are shown for four values of the solar zenith angle.

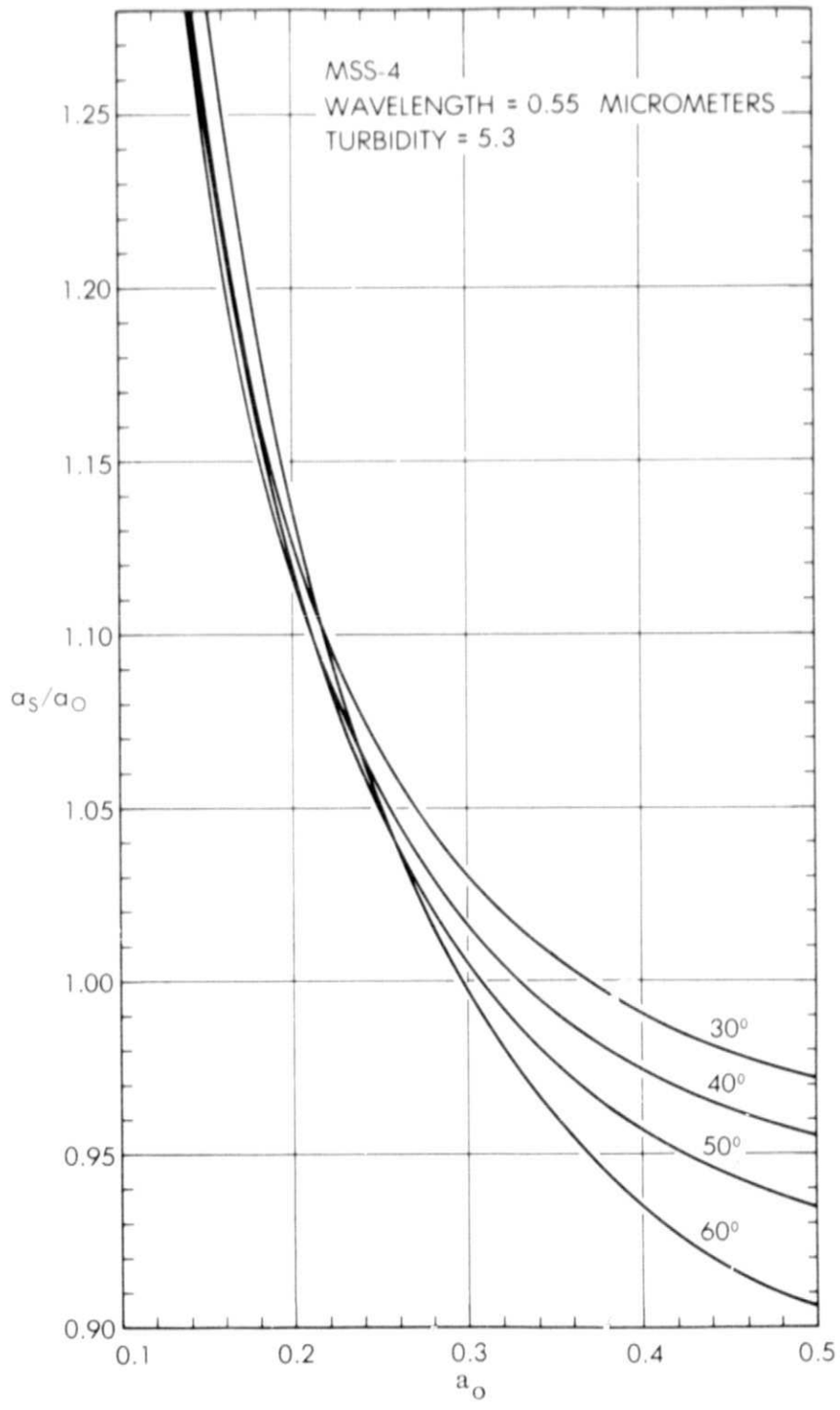

Fig. 6. The space reflectivity to ground reflectivity ratios a_s/a_0 vs ground reflectivity a_0, Band MSS-4, turbidity 5.3. The parametric curves are shown for four values of the solar zenith angle.

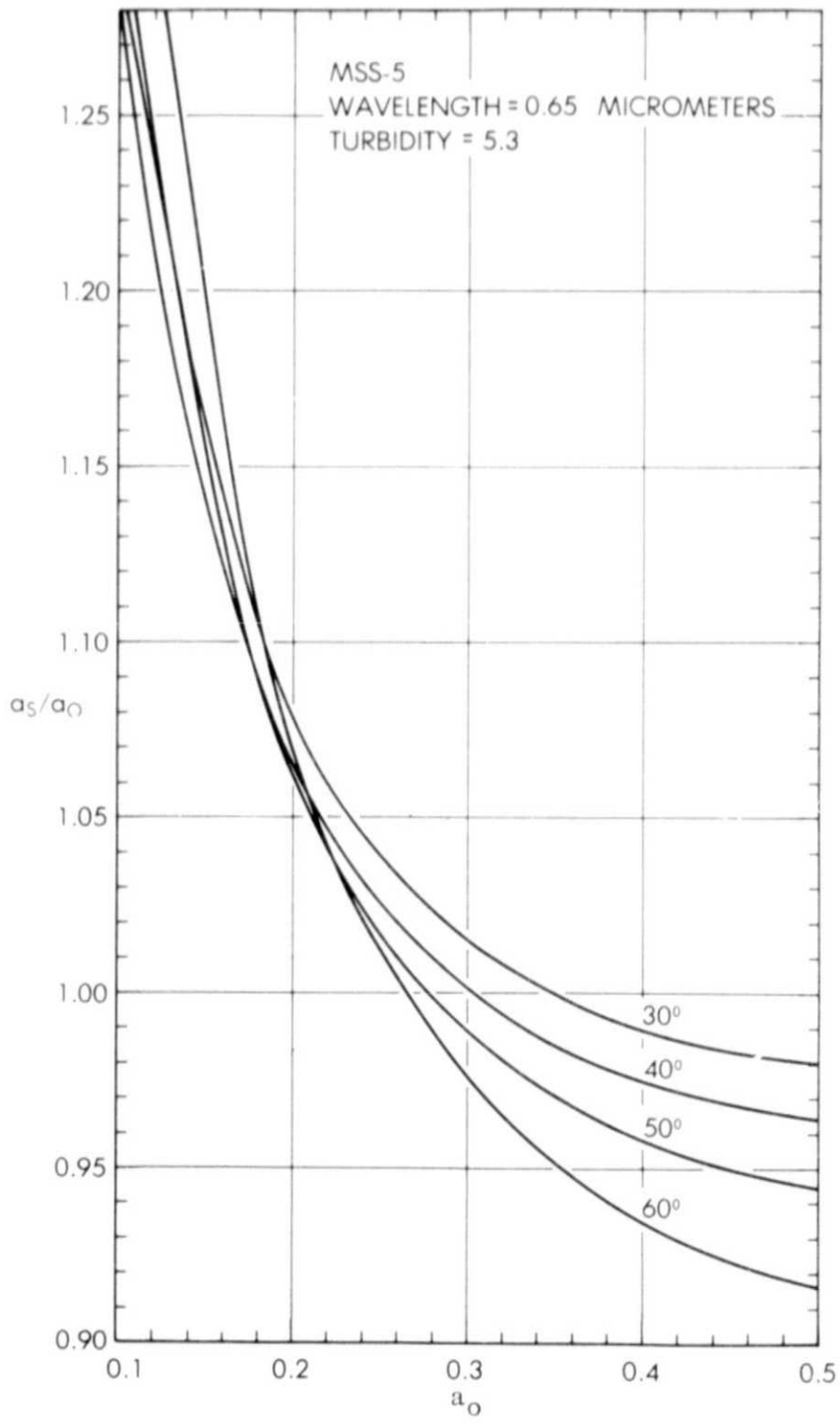

Fig. 7. The space reflectivity to ground reflectivity ratios a_s / a_0 vs ground reflectivity a_0, Band MSS-5, turbidity 5.3. The parametric curves are shown for four values of the solar zenith angle.

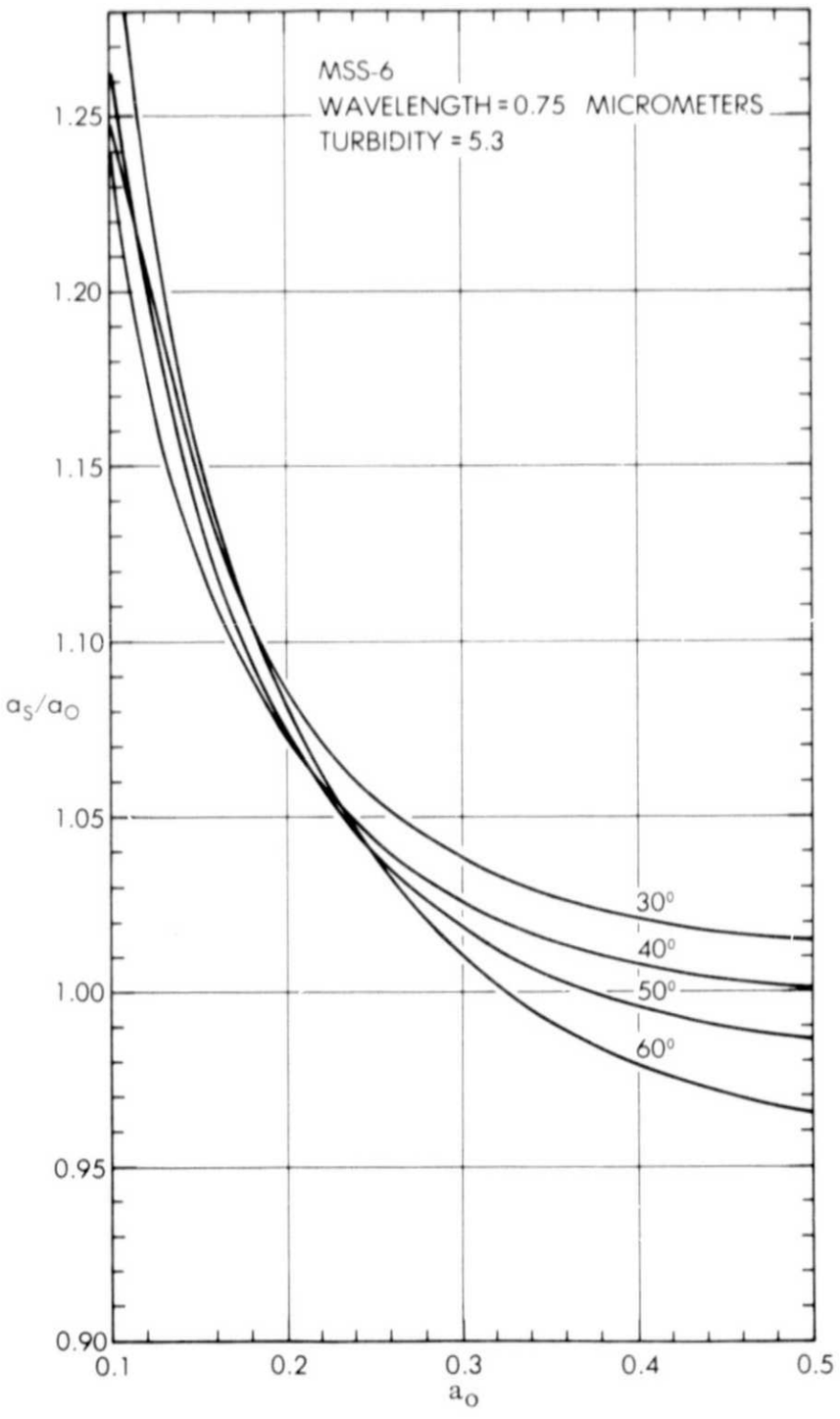

Fig. 8. The space reflectivity to ground reflectivity ratios a_s/a_0 vs ground reflectivity a_0, Band MSS-6, turbidity 5.3. The parametric curves are show for four values of the solar zenith angle.

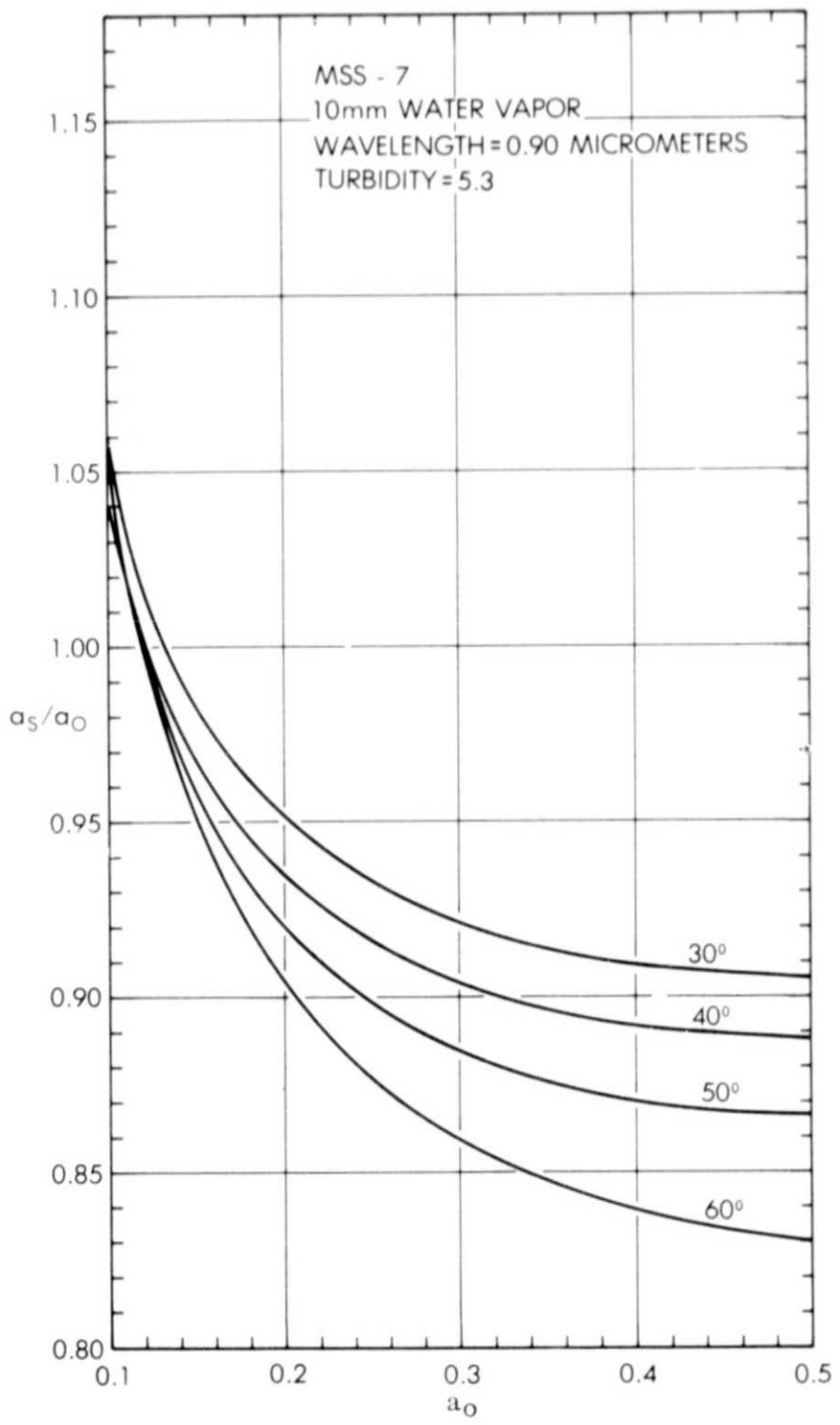

Fig. 9. The space reflectivity to ground reflectivity ratios a_s/a_0 vs ground reflectivity a_0, Band MSS-7, turbidity 5.3, water vapor 10 mm. The parametric curves are shown for four values of the solar zenith angle.

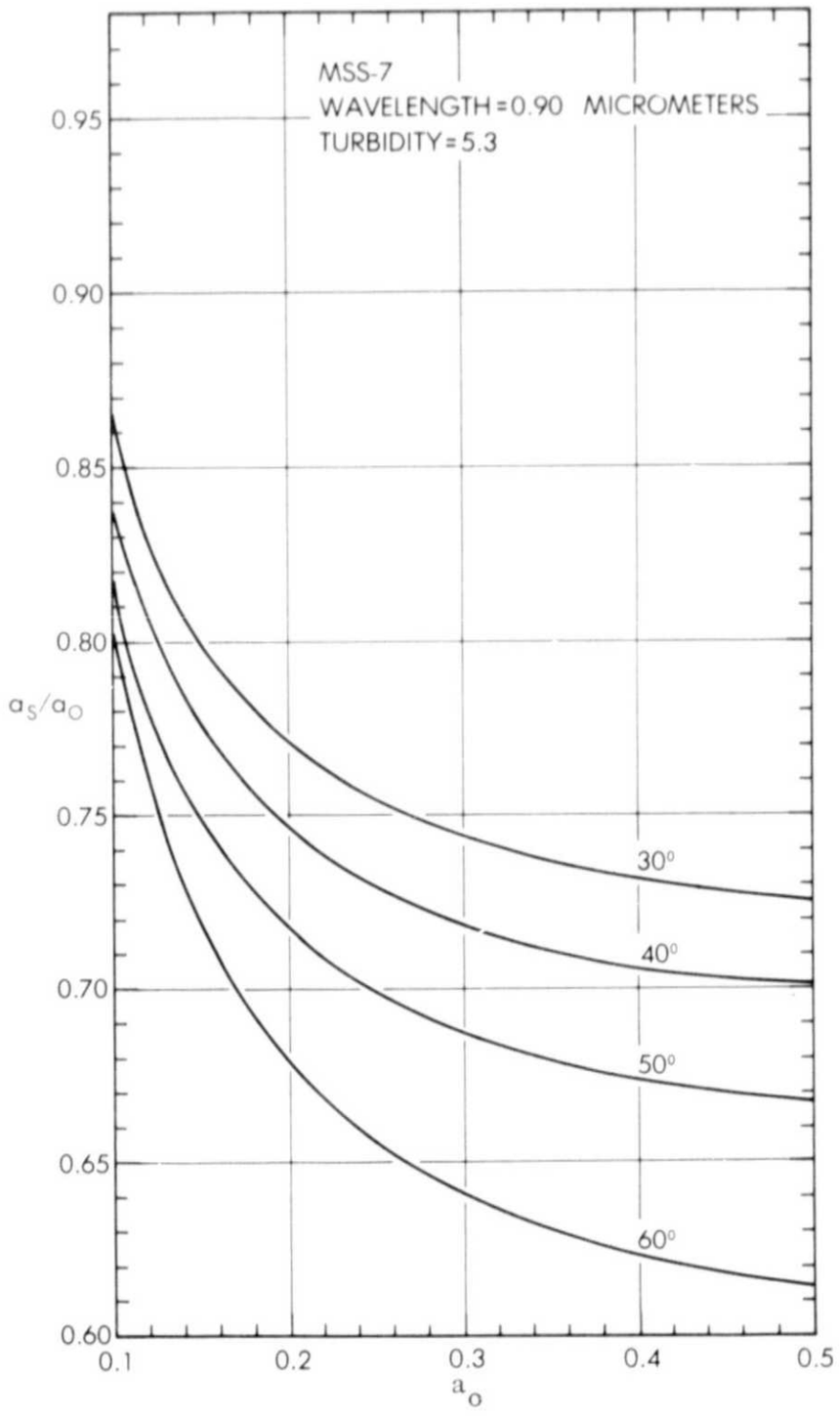

Fig. 10. The space reflectivity to ground reflectivity ratios a_s/a_0 vs ground reflectivity a_0, Band MSS-7, turbidity 5.3, water vapor 29 mm. The parametric curves are shown for four values of the solar zenith angle.

Table 1

Band	Wavelengths Micrometers	Color	LANDSAT-1 Radiance mw/cm²sr		LANDSAT-2 Radiance mw/cm²sr		Solar Spectral Irradiance in the Band (at 1 AU) mw/cm²
			0-Level	Top Level	0-Level	Top Level	
MSS-4	0.5-0.6	Green-yellow	0	2.48	0.10	2.10	17.70
MSS-5	0.6-0.7	Orange-red	0	2.00	0.07	1.56	15.15
MSS-6	0.7-0.8	Red-infrared	0	1.76	0.07	1.40	12.37
MSS-7	0.8-1.1	Infrared	0	4.60	0.14	4.15	24.91

Table 2. Reflectivities (percent) of two areas near the Colorado River, Mexico

	LANDSAT 1										LANDSAT 2											
	ID 193-17290 February 11, 1975 Solar Zenith 57.50°					ID 500-17254 April 24, 1975 Solar Zenith 35.82°					ID 2065-17332 March 28, 1975 Solar Zenith 42.19°					ID 2083-7333 April 15, 1975 Solar Zenith 36.44°					ID 2101-7332 May 3, 1975 Solar Zenith 33.00°				
	Southwest of Colorado River																					
MSS	Turbidity = 3.3			Turbidity = 5.3		Turbidity = 3.3			Turbidity = 5.3		Turbidity = 3.3			Turbidity = 5.3		Turbidity = 3.3			Turbidity = 5.3		Turbidity = 3.3		Turbidity = 5.3		Turbidity = 3.3	Turbidity = 5.3
	a_s	a_s/a_o	a_o	a_s/a_o	a_o	a_s	a_s/a_o	a_o	a_s/a_o	a_o	a_s	a_s/a_o	a_o	a_s/a_o	a_o	a_s	a_s/a_o	a_o	a_s/a_o	a_o	a_s	a_s/a_o	a_o	a_s/a_o	a_o	Average a_o	Average a_o
4	28.4	0.99	28.7	1.01	28.1	32.0	1.00	32.0	1.01	31.7	28.5	1.00	28.5	1.03	27.7	28.7	1.01	28.4	1.04	27.6	29.3	1.01	29.0	1.04	28.2	29.3	28.7
5	30.0	0.96	31.2	0.98	30.6	–	–	–	–	–	30.9	0.98	31.5	0.99	31.2	30.9	0.99	31.2	1.00	30.9	31.7	0.99	32.0	1.01	31.4	31.5	31.0
6	30.6	1.00	30.6	1.01	30.3	34.3	1.01	34.0	1.02	33.6	34.0	1.01	33.7	1.02	33.3	33.2	1.01	32.9	1.02	32.5	34.6	1.01	34.3	1.03	33.6	33.1	32.7
7a	33.0	0.86	38.4	0.85	38.8	36.6	0.90	40.7	0.90	40.7	37.1	0.89	41.7	0.89	41.7	35.2	0.90	39.1	0.90	39.1	37.6	0.90	41.8	0.90	41.8	40.3	40.4
7b	33.0	0.64	51.6	0.63	52.4	36.6	0.72	50.8	0.72	50.8	37.1	0.70	53.0	0.70	53.0	35.2	0.71	49.6	0.71	49.6	37.6	0.72	52.2	0.72	52.2	51.4	51.6
	Northeast of Colorado River																										
4	27.2	1.00	27.2	1.03	26.4	29.1	1.01	28.8	1.03	28.3	26.3	1.02	25.8	1.05	25.0	25.9	1.03	25.1	1.06	24.4	26.0	1.03	25.2	1.07	24.3	26.4	25.7
5	34.4	0.95	36.2	0.95	36.2	37.4	0.98	38.2	0.99	37.8	34.3	0.97	35.4	0.98	35.0	33.9	0.98	34.6	0.99	34.2	33.9	0.98	34.6	1.00	33.9	35.8	35.4
6	35.3	0.99	35.7	0.99	35.7	38.4	1.01	38.0	1.01	38.0	39.4	1.00	39.4	1.01	39.0	37.7	1.01	37.3	1.01	37.3	38.1	1.01	37.7	1.02	37.4	37.6	37.5
7a	39.3	0.85	46.2	0.84	46.8	40.7	0.89	45.7	0.90	45.2	42.0	0.89	47.2	0.88	47.7	39.3	0.90	43.7	0.90	43.7	40.0	0.90	44.4	0.90	44.4	45.4	45.6
7b	39.3	0.63	62.4	0.62	63.4	40.7	0.71	57.3	0.71	57.3	42.0	0.70	60.0	0.69	60.9	39.3	0.71	55.4	0.71	55.4	40.0	0.72	55.6	0.72	55.6	58.1	58.5

a. 10 mm water vapor assumption

b. 29 mm water vapor assumption

Table 2. Reflectivities (percent) of two areas near the Colorado River, Mexico

Table 3

Sahel, 28 December 1973, ID 1523-09331, Solar Zenith Angle 50.6°

	Dark Ranch			Ranch			Overgrazed		
	a_s	a_s/a_o	a_o	a_s	a_s/a_o	a_o	a_s	a_s/a_o	a_o
MSS-4	25.4	1.02	24.9	27.2	1.00	27.2	29.2	0.99	29.5
-5	29.7	0.97	30.6	32.5	0.97	33.5	37.5	0.96	39.1
-6	30.5	1.01	30.2	34.1	1.00	34.1	40.4	0.99	40.8
-7	36.2	0.87	41.6	40.0	0.87	46.0	46.6	0.87	53.6

Sahel, 9 November 1973, ID 1109-09363, Solar Zenith Angle 43°

	Dark Ranch			Ranch			Overgrazed		
	a_s	a_s/a_o	a_o	a_s	a_s/a_o	a_o	a_s	a_s/a_o	a_o
MSS-4	24.9	1.03	24.2	27.1	1.01	26.8	30.1	0.99	30.4
-5	28.4	0.99	28.7	33.7	0.97	34.7	39.0	0.96	40.6
-6	29.0	1.02	28.4	34.6	1.01	34.3	41.1	1.00	41.1
-7	34.4	0.89	38.7	40.3	0.89	45.3	47.8	0.88	54.3

Sinai, 2 January 1973, ID 1163-07483, Solar Zenith Angle 61.5°

	Site 1			Site 2			Site 3		
	a_s	a_s/a_o	a_o	a_s	a_s/a_o	a_o	a_s	a_s/a_o	a_o
MSS-4	27.8	0.99	28.1	29.6	0.97	30.5	36.8	0.93	39.6
-5	34.5	0.94	36.7	36.8	0.94	39.1	45.6	0.95	45.0
-6	38.6	0.98	39.4	39.5	0.98	40.3	47.5	0.97	49.0
-7	46.7	0.84	55.6	47.5	0.84	56.5	56.3	0.84	67.0

Negev, 2 January 1973, ID 1163-07483, Solar Zenith Angle 38.9°

	Site 1			Site 2			Site 3		
	a_s	a_s/a_o	a_o	a_s	a_s/a_o	a_o	a_s	a_s/a_o	a_o
MSS-4	18.6	1.13	16.5	23.4	1.05	22.8	31.0	1.00	31.0
-5	17.0	1.07	15.9	24.0	1.01	23.8	36.8	0.97	37.9
-6	20.9	1.05	19.9	27.7	1.02	27.2	38.7	1.01	38.3
-7	27.6	0.90	30.7	34.9	0.89	39.2	46.3	0.89	52.0

Table 3

Sahel, 28 December 1973, ID 1523-09331, Solar Zenith Angle 50.6°

	Dark Ranch			Ranch			Overgrazed		
	a_s	a_s/a_o	a_o	a_s	a_s/a_o	a_o	a_s	a_s/a_o	a_o
MSS-4	25.4	1.02	24.9	27.2	1.00	27.2	29.2	0.99	29.5
-5	29.7	0.97	30.6	32.5	0.97	33.5	37.5	0.96	39.1
-6	30.5	1.01	30.2	34.1	1.00	34.1	40.4	0.99	40.8
-7	36.2	0.87	41.6	40.0	0.87	46.0	46.6	0.87	53.6

Sahel, 9 November 1973, ID 1109-09363, Solar Zenith Angle 43°

	Dark Ranch			Ranch			Overgrazed		
	a_s	a_s/a_o	a_o	a_s	a_s/a_o	a_o	a_s	a_s/a_o	a_o
MSS-4	24.9	1.03	24.2	27.1	1.01	26.8	30.1	0.99	30.4
-5	28.4	0.99	28.7	33.7	0.97	34.7	39.0	0.96	40.6
-6	29.0	1.02	28.4	34.6	1.01	34.3	41.1	1.00	41.1
-7	34.4	0.89	38.7	40.3	0.89	45.3	47.8	0.88	54.3

Sinai, 2 January 1973, ID 1163-07483, Solar Zenith Angle 61.5°

	Site 1			Site 2			Site 3		
	a_s	a_s/a_o	a_o	a_s	a_s/a_o	a_o	a_s	a_s/a_o	a_o
MSS-4	27.8	0.99	28.1	29.6	0.97	30.5	36.8	0.93	39.6
-5	34.5	0.94	36.7	36.8	0.94	39.1	45.6	0.95	45.0
-6	38.6	0.98	39.4	39.5	0.98	40.3	47.5	0.97	49.0
-7	46.7	0.84	55.6	47.5	0.84	56.5	56.3	0.84	67.0

Negev, 2 January 1973, ID 1163-07483, Solar Zenith Angle 38.9°

	Site 1			Site 2			Site 3		
	a_s	a_s/a_o	a_o	a_s	a_s/a_o	a_o	a_s	a_s/a_o	a_o
MSS-4	18.6	1.13	16.5	23.4	1.05	22.8	31.0	1.00	31.0
-5	17.0	1.07	15.9	24.0	1.01	23.8	36.8	0.97	37.9
-6	20.9	1.05	19.9	27.7	1.02	27.2	38.7	1.01	38.3
-7	27.6	0.90	30.7	34.9	0.89	39.2	46.3	0.89	52.0

Table 3 (Continued)

Libyan Desert, 14 February 1975, ID 2023-08244, Solar Zenith Angle 52.6°

	Sandy			Non-Sandy		
	a_s	a_s/a_o	a_o	a_s	a_s/a_o	a_o
MSS-4	38.6	0.95	40.6	31.9	0.97	32.9
-5	50.8	0.94	54.0	39.2	0.95	41.3
-6	55.8	0.98	56.9	43.3	0.99	43.7
-7	57.7	0.86	67.1	45.5	0.86	52.9

Libyan Desert, 28 January, 1973 ID 1189-08361, Solar Zenith Angle 54.6°

	Sandy			Non-Sandy		
	a_s	a_s/a_o	a_o	a_s	a_s/a_o	a_o
MSS-4	44.1	0.93	47.4	36.8	0.95	38.7
-5	53.8	0.93	57.8	43.6	0.94	46.4
-6	53.2	0.98	54.3	43.5	0.99	43.9
-7	57.2	0.86	66.5	47.1	0.86	54.8

Afghanistan and Kara Kum, USSR, 2 October 1972, ID 1071-05513, Solar Zenith Angle 47.1°

	Afghanistan Overgrazed			Kara Kum Not Overgrazed		
	a_s	a_s/a_o	a_o	a_s	a_s/a_o	a_o
MSS-4	29.9	0.99	30.2	25.7	1.02	25.2
-5	32.9	0.97	33.9	27.1	0.99	27.4
-6	34.0	1.00	34.0	27.7	1.02	27.2
-7	39.7	0.88	45.1	33.0	0.88	37.5

Persian Gulf, 9 February 1973, ID 1201-06184, Solar Zenith Angle 52.0°

	Sandy 54.5°E 27°N			Dark Sea			Dust Storm Over Sea		
	a_s	a_s/a_o	a_o	a_s	a_s/a_o	a_o	a_s	a_s/a_o	a_o
MSS-4	59.6	0.92	64.8	23.3	1.04	22.4	33.4	0.96	34.8
-5	63.2	0.93	68.0	17.8	1.05	17.0	29.7	0.97	30.6
-6	58.1	0.98	59.3	14.7	1.11	13.2	25.3	1.02	24.8
-7	57.5	0.86	66.9	13.0	0.93	14.0	23.8	0.89	26.7

Table 3 (Continued)

Libyan Desert, 14 February 1975, ID 2023-08244, Solar Zenith Angle 52.6°

	Sandy			Non-Sandy		
	a_s	a_s/a_o	a_o	a_s	a_s/a_o	a_o
MSS-4	38.6	0.95	40.6	31.9	0.97	32.9
-5	50.8	0.94	54.0	39.2	0.95	41.3
-6	55.8	0.98	56.9	43.3	0.99	43.7
-7	57.7	0.86	67.1	45.5	0.86	52.9

Libyan Desert, 28 January, 1973 ID 1189-08361, Solar Zenith Angle 54.6°

	Sandy			Non-Sandy		
	a_s	a_s/a_o	a_o	a_s	a_s/a_o	a_o
MSS-4	44.1	0.93	47.4	36.8	0.95	38.7
-5	53.8	0.93	57.8	43.6	0.94	46.4
-6	53.2	0.98	54.3	43.5	0.99	43.9
-7	57.2	0.86	66.5	47.1	0.86	54.8

Afghanistan and Kara Kum, USSR, 2 October 1972, ID 1071-05513, Solar Zenith Angle 47.1°

	Afghanistan Overgrazed			Kara Kum Not Overgrazed		
	a_s	a_s/a_o	a_o	a_s	a_s/a_o	a_o
MSS-4	29.9	0.99	30.2	25.7	1.02	25.2
-5	32.9	0.97	33.9	27.1	0.99	27.4
-6	34.0	1.00	34.0	27.7	1.02	27.2
-7	39.7	0.88	45.1	33.0	0.88	37.5

Persian Gulf, 9 February 1973, ID 1201-06184, Solar Zenith Angle 52.0°

	Sandy 54.5°E 27°N			Dark Sea			Dust Storm Over Sea		
	a_s	a_s/a_o	a_o	a_s	a_s/a_o	a_o	a_s	a_s/a_o	a_o
MSS-4	59.6	0.92	64.8	23.3	1.04	22.4	33.4	0.96	34.8
-5	63.2	0.93	68.0	17.8	1.05	17.0	29.7	0.97	30.6
-6	58.1	0.98	59.3	14.7	1.11	13.2	25.3	1.02	24.8
-7	57.5	0.86	66.9	13.0	0.93	14.0	23.8	0.89	26.7

Table 3 (Continued)

Sinai, 22 October 1972, ID 1091-07482, Solar Zenith Angle 38.9°

	Site 1			Site 2			Site 3		
	a_s	a_s/a_o	a_o	a_s	a_s/a_o	a_o	a_s	a_s/a_o	a_o
MSS-4	31.3	0.99	31.6	34.0	0.98	34.7	37.3	0.97	38.5
-5	39.9	0.97	41.1	44.1	0.97	45.5	46.9	0.96	48.9
-6	39.5	1.00	39.5	43.6	1.00	43.6	45.4	1.00	45.4
-7	41.8	0.89	47.0	45.5	0.89	51.1	48.1	0.89	54.0

Negev, 22 October 1972, ID 1091-07482, Solar Zenith Angle 49.0°

	Site 1			Site 2			Site 3		
	a_s	a_s/a_o	a_o	a_s	a_s/a_o	a_o	a_s	a_s/a_o	a_o
MSS-4	20.2	1.09	18.5	26.3	1.01	26.0	30.5	0.99	30.8
-5	21.2	1.02	20.8	31.5	0.97	32.3	36.0	0.96	37.5
-6	21.1	1.04	20.3	31.0	1.01	30.7	35.2	1.00	35.2
-7	24.2	0.89	27.2	34.2	0.88	38.9	37.9	0.88	43.1

Tip of Sinai, 15 September 1972, ID 1054-07433, Solar Zenith Angle 36.5°

	Red Sand		
	a_s	a_s/a_o	a_o
MSS-4	31.8	1.00	31.8
-5	38.0	0.97	39.2
-6	37.0	1.01	36.6
-7	39.5	0.90	43.6

Libyan Desert, 15 February 1975, ID 2024-08293, Solar Zenith Angle 54.0°

	Sandy			Black Rock			Non-Sandy		
	a_s	a_s/a_o	a_o	a_s	a_s/a_o	a_o	a_s	a_s/a_o	a_o
MSS-4	38.0	0.94	40.4	18.7	1.12	16.7	28.6	0.99	28.9
-5	48.1	0.94	51.2	21.2	1.02	20.8	35.3	0.95	37.2
-6	52.3	0.98	53.4	21.7	1.04	20.9	38.9	0.99	39.3
-7	53.9	0.86	62.7	21.1	0.89	23.7	41.4	0.86	48.1

Table 3 (Continued)

Sinai, 22 October 1972, ID 1091-07482, Solar Zenith Angle 38.9°

	Site 1			Site 2			Site 3		
	a_s	a_s/a_o	a_o	a_s	a_s/a_o	a_o	a_s	a_s/a_o	a_o
MSS-4	31.3	0.99	31.6	34.0	0.98	34.7	37.3	0.97	38.5
-5	39.9	0.97	41.1	44.1	0.97	45.5	46.9	0.96	48.9
-6	39.5	1.00	39.5	43.6	1.00	43.6	45.4	1.00	45.4
-7	41.8	0.89	47.0	45.5	0.89	51.1	48.1	0.89	54.0

Negev, 22 October 1972, ID 1091-07482, Solar Zenith Angle 49.0°

	Site 1			Site 2			Site 3		
	a_s	a_s/a_o	a_o	a_s	a_s/a_o	a_o	a_s	a_s/a_o	a_o
MSS-4	20.2	1.09	18.5	26.3	1.01	26.0	30.5	0.99	30.8
-5	21.2	1.02	20.8	31.3	0.97	32.3	36.0	0.96	37.5
-6	21.1	1.04	20.3	31.0	1.01	30.7	35.2	1.00	35.2
-7	24.2	0.89	27.2	34.2	0.88	38.9	37.9	0.88	43.1

Tip of Sinai, 15 September 1972, ID 1054-07433, Solar Zenith Angle 36.5°

	Red Sand		
	a_s	a_s/a_o	a_o
MSS-4	31.8	1.00	31.8
-5	38.0	0.97	39.2
-6	37.0	1.01	36.6
-7	39.5	0.90	43.6

Libyan Desert, 15 February 1975, ID 2024-08293, Solar Zenith Angle 54.0°

	Sandy			Black Rock			Non-Sandy		
	a_s	a_s/a_o	a_o	a_s	a_s/a_o	a_o	a_s	a_s/a_o	a_o
MSS-4	38.0	0.94	40.4	18.7	1.12	16.7	28.6	0.99	28.9
-5	48.1	0.94	51.2	21.2	1.02	20.8	35.3	0.95	37.2
-6	52.3	0.98	53.4	21.7	1.04	20.9	38.9	0.99	39.3
-7	53.9	0.86	62.7	21.1	0.89	23.7	41.4	0.86	48.1

Table 3 (Continued)

Thar Desert, 30 October 1972, ID 1099-05084,
Solar Zenith Angle 49.0°

	Overgrazed			Dark area		
	a_s	a_s/a_o	a_o	a_s	a_s/a_o	a_o
MSS-4	31.4	0.98	32.0	28.2	1.00	28.2
5	36.3	0.96	38.1	30.9	0.97	31.9
6	35.2	1.00	35.2	30.5	1.01	30.2
7	37.7	0.88	42.8	33.5	0.88	38.1

West Coast of Africa, August 9, 1972, ID 1017-11061
Solar Zenith Angle 31.1°

	Sandy Peninsula		
	a_s	a_s/a_o	a_o
MSS-4	36.8	0.99	37.2
5	43.9	0.97	45.3
6	42.1	1.01	41.7
7	44.5	0.90	49.4

Table 3 (Continued)

Thar Desert, 30 October 1972, ID 1099-05084,
Solar Zenith Angle 49.0°

	Overgrazed			Dark area		
	a_s	a_s/a_o	a_o	a_s	a_s/a_o	a_o
MSS-4	31.4	0.98	32.0	28.2	1.00	28.2
5	36.3	0.96	38.1	30.9	0.97	31.9
6	35.2	1.00	35.2	30.5	1.01	30.2
7	37.7	0.88	42.8	33.5	0.88	38.1

West Coast of Africa, August 9, 1972, ID 1017-11061
Solar Zenith Angle 31.1°

	Sandy Peninsula		
	a_s	a_s/a_o	a_o
MSS-4	36.8	0.99	37.2
5	43.9	0.97	45.3
6	42.1	1.01	41.7
7	44.5	0.90	49.4

Table 4. Spectral Reflectivity Measurements of Terrain Components by Exotech-100 LANDSAT Ground-Truth Radiometer and Reflectivities of Sinai and Negev Derived from the Landsat data.

	MSS Band			
	4 0.5-0 6 mμ	5 0.6-0.7 mμ	6 0.7-0.8 mμ	7 0.8-1.1 mμ
Sinai Soil #1, Crumbled	0.32	0.44	0.50	0.54
Plant Debris	0.09	0.13	0.17	0.26
Sinai Soil #1 Crust	0.28	0.35	0.39	0.43
Artemisia Monosperma Young Growth	0.30	0.20	0.47	0.56
Artemisia Monosperma Twigs	0.29	0.21	0.31	0.43
Sinai #1, Oct. 22, 72	0.32	0.41	0.40	0.47
Sinai #1, Jan. 2, 73	0.28	0.37	0.39	0.56
Negev, #1 Oct. 22, 72	0.19	0.21	0.20	0.27
Negev #1, Jan. 2, 73	0.17	0.16	0.20	0.31

Table 4. Spectral Reflectivity Measurements of Terrain Components by Exotech-100 LANDSAT Ground-Truth Radiometer and Reflectivities of Sinai and Negev Derived from the Landsat data.

	MSS Band			
	4 0.5-0.6 mμ	5 0.6-0.7 mμ	6 0.7-0.8 mμ	7 0.8-1.1 mμ
Sinai Soil #1, Crumbled	0.32	0.44	0.50	0.54
Plant Debris	0.09	0.13	0.17	0.26
Sinai Soil #1 Crust	0.28	0.35	0.39	0.43
Artemisia Monosperma Young Growth	0.30	0.20	0.47	0.56
Artemisia Monosperma Twigs	0.29	0.21	0.31	0.43
Sinai #1, Oct. 22, 72	0.32	0.41	0.40	0.47
Sinai #1, Jan. 2, 73	0.28	0.37	0.39	0.56
Negev, #1 Oct. 22, 72	0.19	0.21	0.20	0.27
Negev #1, Jan. 2, 73	0.17	0.16	0.20	0.31

Table 5

Region	Visible Reflectivity	Infrared Reflectivity	Effective Albedo
Sinai #1 Fall	0.32	0.45	0.39
Sinai #1 Winter	0.31	0.52	0.41
Sinai #3 Fall	0.42	0.52	0.47
Sinai #3 Winter	0.42	0.62	0.52
Sahel Winter Overgrazed	0.34	0.48	0.41
Tip of Sinai Fall	0.35	0.41	0.38
Thar desert	0.34	0.41	0.38
West Coast of Africa	0.40	0.48	0.44
Afghanistan	0.31	0.42	0.37
Mexico, Southwest of Colorado	0.30	0.39	0.34
Mexico, Northeast of Colorado	0.30	0.43	0.37

Table 5

Region	Visible Reflectivity	Infrared Reflectivity	Effective Albedo
Sinai #1 Fall	0.32	0.45	0.39
Sinai #1 Winter	0.31	0.52	0.41
Sinai #3 Fall	0.42	0.52	0.47
Sinai #3 Winter	0.42	0.62	0.52
Sahel Winter Overgrazed	0.34	0.48	0.41
Tip of Sinai Fall	0.35	0.41	0.38
Thar desert	0.34	0.41	0.38
West Coast of Africa	0.40	0.48	0.44
Afghanistan	0.31	0.42	0.37
Mexico, Southwest of Colorado	0.30	0.39	0.34
Mexico, Northeast of Colorado	0.30	0.43	0.37